Deletion of endoplasmic reticulum stress-responsive co-chaperone p58IPK protects mice from diet-induced steatohepatitis

Bandla, Harikrishna ; Dasgupta, Debanjali ; Mauer, Amy S ; Nozickova, Barbora ; Kumar, Swarup ; Hirsova, Petra ; Graham, Rondell P ; Malhi, Harmeet

DOI: https://doi.org/10.1111/hepr.13052

Deletion of endoplasmic reticulum stress-responsive co-chaperone p58^{IPK} protects mice from diet-induced steatohepatitis

Harikrishna Bandla[1], Debanjali Dasgupta[1], Amy S. Mauer[1], Barbora Nozickova[2], Swarup Kumar[3], Petra Hirsova[1], Rondell P. Graham[4], Harmeet Malhi[1*]

1. Division of Gastroenterology and Hepatology, Mayo Clinic, Rochester, MN
2. Universitatsspital Zurich, 8096, Ramistrasse 100, Zurich, Switzerland
3. Department of Medicine, Saint Vincent Hospital, 123 Summer St, Worcester, MA
4. Department of Laboratory Medicine and Pathology, Mayo Clinic, Rochester, MN

Corresponding author: Harmeet Malhi, M.B.B.S.
Associate Professor of Medicine and Physiology
Mayo Clinic College of Medicine
200 First Street SW
Rochester, MN 55905
Tel: 507 284 0686
Fax: 507 284 0762
Email: malhi.harmeet@mayo.edu

Funding: This work was supported by DK 97178, DK107402 and DK111378 (H.M.), the Robert and Elizabeth Strickland Career Development Award from the Division of Endocrinology (H.M.), the Gilead Sciences Research Scholars Program in Liver Disease (H.M.) and the Palumbo Foundation (H.M.), the Edward C. Kendall Research Fellowship Award (P.H.), and the Mayo Foundation.

Running Head: p58^{IPK} mediates murine NASH

Word Count: 4487
References: 30
Figures: 9
Tables: 1

Abbreviations: ALT, alanine aminotransferase; aSMA, alpha smooth muscle actin; ATF4, Activating Transcription Factor 4, ATF 6α, Activating Transcription Factor 6α; BiP/GRP78, Binding immunoglobulin Protein/Glucose Regulated Protein 78; BMDM, bone marrow-derived macrophages; CARS, coherent anti-Stokes Raman scattering; CLAMS, Comprehensive laboratory animals monitoring system; CHOP, C/EBP homologous protein; eIF2α, Eukaryotic translation initiation factor 2 alpha; EVs, Extracellular vesicles; GCN-2, general control non-derepressible 2/eIF2α kinase 4; IRE1α, Inositol Requiring Enzyme 1α; LPS, lipopolysaccharide; MCP1, monocyte chemotactic protein 1; NAFLD, Nonalcoholic fatty liver disease; NASH, Nonalcoholic steatohepatitis; PKR, Protein Kinase RNA-activated; PERK, PKR like ER Kinase; SHG, second harmonic generation; TNFα, tumor necrosis factor alpha; TRAIL-R2, tumor necrosis factor-related apoptosis-inducing ligand receptor 2; TIMP1, tissue inhibitor of metalloproteinase 1; TNF-related apoptosis inducing ligand-receptor 2, WT, Wild Type.

Keywords: Fatty liver, endoplasmic reticulum stress, hepatocyte apoptosis

Activation of the endoplasmic reticulum stress sensor PERK is a feature of nonalcoholic steatohepatitis (NASH), yet regulators of PERK signaling remain undefined in this context. $P58^{IPK}$ regulates PERK; however, its role in NASH has not been examined. Aim: the aim of this study was to assess the *in vivo* role of $p58^{IPK}$ in the pathogenesis of dietary NASH. Methods: parameters of hepatocyte cell death, liver injury, inflammation, fibrosis, indirect calorimetry and PERK activation were assessed in $p58^{IPK}$ knockout ($p58^{ipk-/-}$) mice and their wildtype littermate controls fed a diet enriched in Fat, Fructose, and Cholesterol (FFC) for 20 weeks. Results: PERK activation was attenuated in FFC-fed $p58^{ipk-/-}$ mice. Accordingly, FFC-fed $p58^{ipk-/-}$ mice demonstrated a reduction in hepatocyte apoptosis and death receptor expression, with a significant reduction in serum alanine transaminase values. Correspondingly, macrophage accumulation and fibrosis were significantly lower in FFC-fed $p58^{ipk-/-}$ mice. Conclusion: we have demonstrated that in an *in vivo* dietary NASH model $p58^{IPK}$ mediates hepatocyte apoptosis and liver injury, likely via PERK phosphorylation. In the absence of $p58^{IPK}$, PERK phosphorylation and NASH are attenuated. Inhibition of hepatic $p58^{IPK}$ may be a future target for NASH therapy.

The incidence of obesity-associated nonalcoholic steatohepatitis (NASH) is rising worldwide, especially in the western world[1] leading to increased interest in understanding the pathophysiology of NASH, with an aim to determine therapeutic approaches to treat the disease. The molecular pathogenesis of NASH supports the view that lipotoxicity, the deleterious consequence of accumulated lipids in hepatocytes, plays a key role in disease development[2]. At a cellular and molecular level lipotoxicity is associated with activation of the endoplasmic reticulum (ER) stress response in the liver[3], though a complete understanding of the role of ER stress signaling cascades during lipotoxicity is lacking. This is partly due to the complex nature of the ER stress response, wherein, multiple divergent signaling pathways are activated simultaneously[4,5]. Furthermore, though the canonical signaling cascades activated by the accumulation of unfolded proteins are well defined, lately, there has been an expansion in our understanding of how individual components of the ER stress response machinery play disparate roles in obesity-associated disorders[6,7]. Some of these proteins have pathophysiologic roles beyond the traditional unfolded protein response-activated signaling pathways, such as, the role of X-box binding protein 1 (XBP-1) in regulating hepatic lipogenesis[8] and bile acid metabolism[9].

The DnaJ family protein p58^{IPK} (DNAJC3) is an important modulator of the ER stress response protein PKR-like ER kinase (PERK) and cytosolic double-stranded RNA-dependent protein kinase (PKR) signaling[10,11]. P58^{IPK} is induced by ER stress, localizes to the ER lumen where a co-chaperone function has been described[12]. Additionally, p58^{IPK} has chaperone-independent and ER stress-independent functions in the regulation of cytosolic proteins. For example, it binds to the kinase domain of PKR, thus preventing its dimerization and activation[13]. P58^{IPK} can also inhibit the additional eukaryotic translation initiation factor 2 alpha (eIF2α) kinase general control non-derepressible 2/eIF2α kinase 4 (GCN-2)[14]. Thus, p58^{IPK} regulates several pathways potentially relevant in the pathogenesis of NASH; yet, the

role of p58^{IPK} in NASH has not been examined. Its role in this process might be critical given its high expression level in the liver[15]. Therefore, the objective of this study was to examine the contribution of p58^{IPK} to NASH in a dietary murine model.

We employed p58^{IPK} knockout (*p58$^{ipk-/-}$*) mice which have been previously described[16] and a dietary model of NASH induced by *ad libitum* feeding of a diet high in fat, fructose, and cholesterol as previously described by us[17]. We report that the activation of PERK was inhibited in FFC-fed *p58$^{ipk-/-}$* mouse livers, indicating that p58^{IPK} is necessary for PERK activation in this chronic dietary stress model. In addition, *p58$^{ipk-/-}$* mice are protected from hepatocyte apoptosis and liver injury. The reduction in liver injury is associated with a decrease in liver inflammation and consequent fibrosis. Thus, we conclude that p58^{IPK} mediates NASH likely by promoting PERK activation which contributes to hepatocyte apoptosis and NASH pathogenesis.

RESULTS

PERK activation is attenuated in FFC-fed *p58$^{ipk-/-}$* mice. We first interrogated activation of PERK phosphorylation in *p58$^{ipk-/-}$* mouse livers in a dietary NASH model. We found that in FFC-fed wildtype mice PERK was phosphorylated; the lack of p58^{IPK} led to significant reduction in PERK phosphorylation (Fig. 1A). In chow-fed and FFC-fed *p58$^{ipk-/-}$* mice, we noted an increase in eIF2α phosphorylation without an increase in PERK phosphorylation implicating one of the other eIF2α kinases in its phosphorylation. Though there was an increase in eIF2α phosphorylation we did not detect an increase in the levels of activating transcription factor 4 (ATF4), which is selectively translated following eIF2α phosphorylation, in FFC-fed *p58$^{ipk-/-}$* mice compared with FFC-fed WT mice. In fact, ATF4 expression was lower in FFC-fed *p58$^{ipk-/-}$* mice compared with FFC-fed WT mice. Similarly, the levels of C/EBP homologous protein (CHOP), which is downstream of ATF4, were lower

in FFC-fed *p58*$^{ipk-/-}$ mice compared with FFC-fed WT mice (Fig. 1B); the lower band is a well-recognized non-specific signal derived from CHOP antibodies[18]. Quantification of CHOP mRNA was consistent with the protein expression data (Fig. 1C). CHOP mRNA expression was induced in FFC-fed WT mice; however, reduced in FFC-fed *p58*$^{ipk-/-}$ mice. To confirm that the reduction in PERK phosphorylation was specific to chronic dietary stress, we induced acute pharmacologic ER stress in wildtype and *p58*$^{ipk-/-}$ mice with intraperitoneal tunicamycin injection. Following tunicamycin injection PERK phosphorylation was unchanged in *p58*$^{ipk-/-}$ mice (Fig. 1D and E), suggesting that the observed reduction in PERK phosphorylation was specific to this dietary NASH model.

Chronic dietary stress due to the FFC diet is known to activate the ER stress response in the liver; therefore we asked if there was differential activation of the inositol requiring enzyme 1 alpha (IRE1α) and activating transcription factor alpha (ATF6α) pathways in the FFC-fed *p58*$^{ipk-/-}$ mice in comparison to FFC-fed WT mice. IRE1α activation was assessed by splicing of its target mRNA, X-box binding protein 1 (XBP-1). Consistent with previous reports, FFC-feeding led to a significant increase in XBP-1 splicing (Fig. 2A); this was attenuated in the FFC-fed *p58*$^{ipk-/-}$ mice. Expression of ATF6α target genes was similarly induced with FFC-feeding in WT mice and remained attenuated in FFC-fed *p58*$^{ipk-/-}$ mice (Fig. 2B and C). These data suggest that FFC-fed *p58*$^{ipk-/-}$ mice livers are resistant to diet-induced ER stress.

***p58*$^{ipk-/-}$ mice are resistant to liver injury.** The liver is a key target organ for dietary obesity-associated tissue injury. Therefore, we next examined the livers of FFC-fed WT and *p58*$^{ipk-/-}$ mice for the development of NASH. Following 20 weeks of FFC-feeding, the liver index (relative liver mass) of FFC-fed *p58*$^{ipk-/-}$ mice demonstrated hepatomegaly which was comparable to the relative liver mass of FFC-fed WT mice, and significantly greater than chow-fed *p58*$^{ipk-/-}$ mice (Fig. 3A). Interestingly, even chow-fed *p58*$^{ipk-/-}$ mice demonstrated

hepatomegaly in comparison with chow-fed WT mice. Therefore, the *p58*$^{ipk-/-}$ mice develop significant hepatomegaly. We have previously demonstrated that this dietary model of obesity-associated NASH is characterized by hepatocyte steatosis, hepatocyte ballooning, liver injury and inflammation, and activation of profibrogenic signaling with prolonged FFC feeding [17]. Therefore, we next undertook histologic assessment of hepatic architecture after 20 weeks of FFC diet feeding. This demonstrated that the FFC-fed WT livers had features of NASH including steatosis, lobular inflammation, and fibrosis (Fig. 3B). Liver of FFC-fed *p58*$^{ipk-/-}$ mice appeared to have diminished hepatic steatosis on H and E images (Fig. 3C); therefore, we performed coherent anti-Stokes Raman scattering (CARS) microscopy for label-free quantification of the triglyceride content (Fig. 3C and D). Consistent with the visual assessment of steatosis reduction, CARS-based quantification demonstrated mild reduction in steatosis between the FFC-fed WT and *p58*$^{ipk-/-}$ mice. Thus the FFC-fed WT and *p58*$^{ipk-/-}$ mice developed comparable hepatomegaly; though there was mild reduction in steatosis in the *p58*$^{ipk-/-}$ mice. Next, we looked at parameters of liver injury by measuring serum alanine aminotransferase (ALT), a marker of hepatocyte injury. Serum ALT was significantly elevated in WT mice fed the FFC diet for 20 weeks (Fig. 3E). In contrast, FFC-fed *p58*$^{ipk-/-}$ mice had a significantly lower ALT value reflecting lesser hepatocyte injury.

Hepatocyte apoptosis is reduced in FFC-fed *p58*$^{ipk-/-}$ mice. Hepatocyte apoptosis is a key determinant of liver injury in NASH, therefore, we next asked if there was a concomitant reduction in apoptosis in the livers of FFC-fed *p58*$^{ipk-/-}$ mice. We found that FFC-feeding led to hepatocyte apoptosis in WT mice (Fig. 4A and B). Apoptosis was significantly lower in FFC-fed *p58*$^{ipk-/-}$ mice. The expression of the death receptors, TNF-related apoptosis inducing ligand-receptor 2 (TRAIL-R2) and Fas, both of which are upregulated in NASH, were correspondingly increased by FFC feeding in WT mice (Fig. 4C and D), and reduced in FFC-

fed *p58*$^{ipk-/-}$ mice. Thus, p58^{IPK} appears to mediate hepatocyte apoptosis in lipotoxicity. In its absence hepatocyte apoptosis and liver injury are reduced.

Liver inflammation is reduced in *p58*$^{ipk-/-}$ mice. Macrophage-mediated activation of the innate immune system is a key feature of liver injury in NASH and correlates with progressive disease. Therefore, we next examined hepatic macrophage accumulation using F4/80 immunohistochemistry. FFC-fed WT mice demonstrated significantly greater accumulation of F4/80 positive macrophages in the liver (Fig. 5A). This was reduced in FFC-fed *p58*$^{ipk-/-}$ mice. Corresponding quantification of F4/80 immunohistochemistry is shown in Fig. 5B. There was a reduction in the mRNA abundance of markers of macrophage accumulation including F4/80 (Fig. 5C) and CD68 (Fig. 5D), and a reduction in the myeloid cell recruiting chemokine monocyte chemotactic protein 1 (MCP-1) (Fig. 5E). Therefore, *p58*$^{ipk-/-}$ mice demonstrate a reduction in liver inflammation compared to FFC-fed WT mice.

Hepatic fibrosis is reduced in *p58*$^{ipk-/-}$ mice. Chronic liver injury and inflammation result in hepatic fibrosis. Therefore, we asked if the reduction in liver injury and inflammation in the *p58*$^{ipk-/-}$ mice was associated with a reduction in hepatic fibrosis. The expression of alpha smooth muscle actin (aSMA), a marker of activated hepatic stellate cells, was increased in FFC-fed WT mice in comparison with chow-fed WT and *p58*$^{ipk-/-}$ mice (Fig. 6A). However, aSMA expression was significantly lower in the FFC-fed *p58*$^{ipk-/-}$mice (Fig 6A and C). To complement the immunohistologic analysis we performed second harmonic generation (SHG) microscopy for the quantification of collagen fibrils (Fig. 6B and D). SHG microscopy demonstrated significant collagen deposition in FFC-fed WT livers, which was reduced in FFC-fed *p58*$^{ipk-/-}$ liver, consistent with the aSMA immunohistochemistry. Furthermore, the mRNA expression of pro-fibrogenic genes, such as collagen 1a1 and tissue inhibitor of metalloproteinases 1 (TIMP1), was in keeping with the histologic analyses (Fig.

6E and F). Thus, hepatic fibrosis is reduced in FFC-fed *p58*$^{ipk-/-}$ mice, a likely consequence of the reduction in liver injury and inflammation.

***P58*$^{ipk-/-}$ mice are resistant to diet-induced obesity.** *P58*$^{ipk-/-}$ mice were smaller than age-matched WT littermate controls at the start and completion of the feeding study (Fig. 7A and B). When fed the FFC diet, WT mice gained weight; however, *p58*$^{ipk-/-}$ mice remained resistant to weight gain, with terminal body mass of FFC-fed *p58*$^{ipk-/-}$ mice comparable to chow-fed *p58*$^{ipk-/-}$ mice (Fig. 7B). The resistance to weight gain was not due to a reduction in food intake. In fact, FFC-fed *p58*$^{ipk-/-}$ mice consumed more food than FFC-fed WT mice (Fig. 7C and D). Greater food consumption is likely secondary to the known pancreatic beta cell failure with resultant diabetes in *p58*$^{ipk-/-}$ mice as previously reported[16]. The *p58*$^{ipk-/-}$ mice had comparable fasting hyperglycemia regardless of diet (Fig. 7E). Further characterization of the metabolic effects of FFC-feeding demonstrated comparable hypercholesterolemia in FFC-fed WT and *p58*$^{ipk-/-}$ mice (Fig. 7F) with corresponding increases in levels of HDL cholesterol and the LDL/VLDL cholesterol concentrations (Fig. 7G and H). We next investigated differences in energy expenditure in these mice by indirect calorimetry. Resting and active energy expenditure was higher in FFC-fed *p58*$^{ipk-/-}$ mice in comparison to FFC-fed WT mice (Fig. 8A and B). Similarly, total energy expenditure was also higher in FFC-fed *p58*$^{ipk-/-}$ mice in comparison to FFC-fed WT (Fig. 8C). The respiratory exchange ratio was higher in the FFC-fed *p58*$^{ipk-/-}$ mice (Fig. 8D) in the fasted state. Activity (Fig. 8E), ambulation (Fig. 8F) and rearing (Fig. 8G) counts, all reflective of physical activity, were not statistically significantly different among groups. Thus, the FFC-fed *p58*$^{ipk-/-}$ mice remain resistant to weight gain in spite of increased food intake likely due to increased energy expenditure in comparison to FFC-fed WT mice. Furthermore, they demonstrate profound fasting hyperglycemia. WT and *p58*$^{ipk-/-}$ mice develop hypercholesterolemia upon FFC feeding, consistent with the known effects of this diet.

Proinflammatory macrophage responses are intact in *p58$^{ipk-/-}$* mice. Due to the importance of macrophages in hepatic inflammation and fibrosis and our observation of reduced macrophage accumulation in FFC-fed *p58$^{ipk-/-}$* mice, we asked whether macrophage inflammatory responses were intact in *p58$^{ipk-/-}$* mice. To answer this we isolated bone marrow-derived macrophages (BMDM) from WT and *p58$^{ipk-/-}$* mice and examined their activation upon treatment with lipopolysaccharide (LPS). We found that proinflammatory responses to LPS were not mitigated in *p58$^{ipk-/-}$* BMDM (Fig. 9A). Similarly, macrophage migratory capacity was intact in *p58$^{ipk-/-}$* BMDM (Fig. 9B).

DISCUSSION

The principal findings of this study have elucidated a role for p58^{IPK} in the development of murine NASH by demonstrating that in a dietary NASH model: i) PERK phosphorylation is attenuated in *p58$^{ipk-/-}$* mice; ii) FFC-fed *p58$^{ipk-/-}$*mice are protected from hepatocyte apoptosis, liver injury and inflammation; and iii) macrophage proinflammatory and migratory responses are intact in the absence of p58^{IPK}. These data elucidate a novel role for p58^{IPK} in the pathogenesis of hepatocellular injury in dietary obesity-associated NASH.

P58^{IPK} (*DNAJC3*) was identified as an ER stress-induced gene[10] in cells treated with the pharmacologic ER stress inducers tunicamycin or thapsigargin. Enforced overexpression of p58^{IPK} leads to inhibition of phosphorylation of eIF2α and reduced translation of ATF4. In isolated cells, overexpression of p58^{IPK} does not protect against ER stress-induced apoptosis; however, its silencing sensitizes to apoptosis[12]. Additional *in vitro* data have demonstrated that p58^{IPK} regulates the eIF2α kinases PERK, PKR and GCN2 by inhibiting their phosphorylation[14,19]. However, its role *in vivo* remains incompletely defined. P58^{IPK} is expressed in all tissues and its expression levels are known to be high in the pancreas and the liver[15]. Mice lacking p58^{IPK} develop glucosuria, hyperglycemia, and hypoinsulinemia due to apoptotic cell death of pancreatic islet cells; however, they are not insulin resistant[16]. In

keeping with these observations, monogenic type I diabetes is described in humans with homozygous DNAJC3 deletion[20]. However, heretofore, the effects of p58^{IPK} loss have not been examined in the liver. Furthermore, its contribution to the pathogenesis of NASH is unknown.

Using a dietary model of NASH we found that the FFC-diet led to body weight gain in WT mice with concomitant hyperglycemia; however, *p58$^{ipk-/-}$* mice remained resistant to obesity in spite of greater food intake. This is likely due to the increased resting and active energy expenditure observed in *p58$^{ipk-/-}$* mice. The increase in energy expenditure is likely due to the known metabolic effects of type I diabetes, as reported by others[21-23], where resting energy expenditure and food-induced thermogenesis are both increased in type I diabetics leading to tissue catabolism. However, the livers of *p58$^{ipk-/-}$* mice were not equally resistant to diet-induced steatosis. Indeed, the liver weight/body weight ratio of FFC-fed *p58$^{ipk-/-}$* mice was similar to that of FFC-fed WT mice. Unbiased quantification of liver fat demonstrated only a mild reduction in liver fat content in FFC-fed *p58$^{ipk-/-}$* mice. In contrast, we found a significant reduction in liver injury, inflammation, and consequent fibrosis in FFC-fed *p58$^{ipk-/-}$* mice. These data suggest a cell autonomous role for p58^{IPK} in promoting hepatocyte apoptosis and injury, as hepatocyte apoptosis is an important pathogenic event in NASH development [24]. Indeed, we found that the expression of death receptors TRAIL-R2 and Fas was reduced in FFC-fed *p58$^{ipk-/-}$* mice as was hepatocyte apoptosis. The reduction in hepatocyte apoptosis maybe a consequence of lower CHOP expression in the livers of FFC-fed *p58$^{ipk-/-}$* mice, and possibly increased energy expenditure with a minimal reduction in hepatic steatosis. This could be verified further with hepatocyte-specific conditional knockout mice; however, mice with a conditional deletion of p58^{IPK} have not yet been developed.

In the absence of conditionally deleted p58^{IPK} mice we dissected the contribution of macrophages in our dietary model as macrophages are key mediators of the sterile

inflammatory response that is a characteristic feature of liver injury and inflammation in NASH[25]. We noted a reduction in macrophage accumulation in the livers of FFC-fed *p58*$^{ipk-/-}$ mice, in keeping with other pharmacologic and genetic models that demonstrate a reduction in liver inflammation with amelioration of liver injury[17,26]. The proinflammatory activation and migration responses of *p58*$^{ipk-/-}$ bone marrow derived macrophages toward lipopolysaccharide were intact, suggesting that hepatocyte p58^{IPK} was likely important in mediating hepatocyte injury. Therefore, the observed reduction in macrophage accumulation would be secondary to the reduction in liver injury. We also noted a reduction in hepatic fibrosis, a consequence of reduced injury and inflammation.

High fat diet feeding is known to activate the ER stress pathways including PERK signaling[27]. In keeping with the observations of others, we found that FFC-feeding activated PERK as demonstrated by increased PERK phosphorylation. However, FFC-fed *p58*$^{ipk-/-}$ mice demonstrated a significant reduction in PERK phosphorylation. Though FFC-feeding induced eIF2α phosphorylation, the levels of phosphorylated eIF2α were higher in the FFC-fed *p58*$^{ipk-/-}$mice than FFC-fed WT mice. This occurred in the absence of significant PERK phosphorylation, implicating one of the other eIF2α kinases in this process. Downstream of the phosphorylation of eIF2α, we did not observe an increase in ATF4 induction, in fact ATF4 expression was lower in FFC-fed *p58*$^{ipk-/-}$ mice compared to WT mice. In keeping with this, CHOP protein expression and mRNA abundance was lower in FFC-fed *p58*$^{ipk-/-}$ mice with respect to WT mice. Therefore, we conclude that under chronic dietary stress conditions the FFC-fed *p58*$^{ipk-/-}$ mice are resistant to activation of the ER stress pathways including PERK phosphorylation and CHOP induction; the later possibly mediate a reduction in hepatocyte apoptosis as observed in FFC-fed *p58*$^{ipk-/-}$ mice. This is consistent with previous reports that the PERK/ATF4/CHOP pathway mediates palmitate-induced apoptosis in hepatocytes[28].

The lack of PERK phosphorylation in FFC-fed *p58$^{ipk-/-}$* suggests that there is a novel role for p58^{IPK} in maintaining PERK activation in chronic dietary stress. Though the regulation of eIF2α signaling downstream of PERK activation is well-studied, the regulators of the proximal kinases remain undefined. In this regard the molecular regulation of PERK levels, activation and dephosphorylation remain incompletely understood. Furthermore, though, PERK knockout mice have been described, they uniformly experience neonatal lethality precluding high fat diet feeding to these mice[29]. We found that the *in vivo* reduction of PERK phosphorylation in the FFC-fed dietary model was distinct from the role of p58^{IPK} in pharmacologic ER stress, as *p58$^{ipk-/-}$* mice treated with tunicamycin showed unchanged PERK phosphorylation.

Thus, we conclude that p58^{IPK} promotes liver injury by PERK phosphorylation and activation under conditions of dietary stress. We have not elucidated how p58^{IPK} promotes PERK phosphorylation, such as, stabilization of PERK protein dimers, and this will be an area for future studies. Our data also suggest that inhibition of hepatic p58^{IPK} may be a novel therapeutic target in NASH.

MATERIALS and METHODS

Animal studies. All animal use was approved by the institutional care and animal use committee of the Mayo Clinic and conducted in accordance with the public health policy on the humane use and care of laboratory animals. Previously descried p58^{IPK} knockout mice (*p58$^{ipk-/-}$*) were a gift from Dr. Katz[16]. Twelve-week old male knockout mice and their wildtype (WT) littermate controls were fed either chow or a diet high in saturated fat, fructose and cholesterol (FFC) for 20 weeks. This diet has been previously described by us and recapitulates many cardinal features of human NASH[17]. Overall, 14 mice were fed chow and 16 mice FFC diet. Out of 14 mice chow-fed 6 were WT and 8 were *p58$^{ipk-/-}$* and out of 16

FFC-fed mice 8 were WT and 8 were *p58*$^{ipk-/-}$. Mice were co-housed in specific pathogen free facilities and had unrestricted access to food and water. All the mice were on their respective diets for 20 weeks before euthanasia. Total body weight was measured using a standard balance. Following euthanasia, blood was collected for serum alanine aminotransferase measurement. Liver was excised, weighed, and apportioned for downstream analyses, including RNA extraction, protein extraction, formalin fixation and paraffin embedding for histology, and cryo-sectioning.

Fasting blood glucose measurements. Mice were fasted for 8 hours before measuring the blood glucose. Blood glucose was measured using blood glucose meter (Assure® 4 manufactured by ARKRAY™). Blood was collected from the tail vein and the strips provided in the kit were used to measure blood glucose.

Indirect calorimetry and physical activity. Oxygen consumption (VO_2), carbon dioxide production (VCO_2), and food intake were measured for 24 hours under both fed and fasted conditions using a comprehensive laboratory animal monitoring system (CLAMS) equipped with an Oxymax Open Circuit Calorimeter (Columbus Instruments, Columbus, OH) in 4 mice per group at week 16 of dietary feeding. VO_2 and VCO_2 were used to calculate energy expenditure (kcal/kg/hr). The habitual physical activity of individual mice was measured in the horizontal (ambulation) and vertical (rearing) planes for a 48-hour period in the CLAMS using photocells.

Biochemical assays and multimodal microscopy. Serum ALT levels were measured using a commercially available veterinary scanner (Vet Scan 2, Abaxis). Cholesterol levels were measured using a commercially available assay (Cholesterol/Cholesteryl Ester Quantification Kit II, K623-100, BioVision). Cholesterol concentrations in High Density Lipoprotein (HDL) and Low Density Lipoprotein/ Very Low Density Lipoprotein (LDL/VLDL) were measured

using a commercially available assay (EnzyChrom™ AF HDL and LDL/VLDL Assay Kit, E2HL-100) by colorimetric procedure. Coherent Anti-stokes Raman Scattering (CARS) and Second Harmonic Generation (SHG) microscopy were performed on label-free liver cryo sections (7 µm) imaged on a two photon confocal microscope FluoView FV1000 MPE (Olympus America, Center Valley, PA) using the CARS and SHG applications as previously described by us[26]. Images were obtained using XLPlanN 25×/1.05w MP objective lens. For quantification, the areas of the CARS (neutral lipid) or SHG (collagen) signal having intensity above the threshold value were calculated using ImageJ (NIH).

Histological analyses. Liver tissues were fixed in neutral buffered formalin, embedded in paraffin and sectioned. Standard Hematoxylin and Eosin stained liver sections were graded according to the NAFLD activity score[30]. Accumulation of extracellular matrix was quantified using Picro-Sirius red staining as previously described by us[26]. The positive areas were captured at 20× magnification on Nikon NIS elements advanced research imaging software attached to Nikon Eclipse TE300 microscope (Nikon, Japan). Quantitative morphometry was performed on the individual images for the Sirius red chromogen. Immunohistochemistry was done following the standard ABC Immunostaining kit (Vector labs) protocol. Briefly, slides were dewaxed using xylene and rehydrated through graded ethanol solutions. Antigen retrieval was performed by heating slides to 95°C in 10 mM sodium citrate buffer, pH 6.0, for 30 minutes. Peroxidase, avidin, biotin and non-specific binding sites in the tissue were blocked. Alpha Smooth muscle actin (aSMA) antibody (Abcam ab124964) and F4/80 antibody (eBioscience, 14-4801-82) at 1:100 dilutions were applied to the tissue and incubated overnight in a humidified chamber at 4°C. After washing in PBS, slides were incubated with biotin-conjugated secondary antibody and streptavidin conjugated to horseradish peroxidase and lastly chromogenic substrate per the manufactures instructions (ABC, Vector Labs). Dehydrated sections were mounted using Permount

mounting media (Sigma). The positive areas were captured at 20× magnification using the Nikon NIS-Elements advanced research imaging software attached to a Nikon Eclipse TE300 microscope (Nikon, Japan) or Zeiss Axio Scope A1 attached to an Axiocam 105 color. Images with uniform settings of magnification, light, and exposure time were used for quantitative image analysis. *In Situ* Cell Death Detection Kit Fluorescein (Roche) was used to detect DNA strand breaks by the TUNEL method in paraformaldehyde fixed 10 μM thick liver cryosections according to the manufacturer's instructions. Nuclei were counterstained with DAPI (Sigma), and quantified by averaging the number of apoptotic nuclei seen in 10 high power fields per sample.

Tunicamycin injection. Three pairs of age-matched WT and *p58ipk*$^{-/-}$ mice were weighed and injected with 2 mg/kg tunicamycin intraperitoneally. One pair of mice was euthanized 4 hours after intraperitoneal tunicamycin injection and 2 pairs were euthanized 6 hours after intraperitoneal tunicamycin injection. Liver tissue was collected as above.

Quantitative PCR. Total RNA was isolated from frozen liver tissue by homogenizing in Trizol reagent using a handheld homogenizer in 1 mL Trizol per 15-20 mg of liver tissue. 300 μL of homogenate was transferred into a new 2 mL Eppendorf tube and 700 μL of Trizol and 1 mL of 100% ethyl alcohol was added. This solution was applied to the RNA isolation column (Zymo-Spin™ IIC Column, Direct-zol™ RNA MiniPrep kit) in a ollection tube (provided by the manufacturer in the Direct-zol™ RNA MiniPrep kit) and the RNA was extracted according to the manufacturer's instructions including a DNase I treatment. RNA was quantified and assessed for quality using a Nano Drop ND1000 (ThermoScientific). Reverse transcription was performed with the iScript cDNA synthesis kit (Bio-Rad). Quantitative real-time PCR (qPCR) reactions were run on the Light Cycler 480 (Roche), using the Light Cycler 480 SYBR Green 1 Master Mix (Roche). Primers are summarized in

table 1. Data are expressed relative to HPRT, which was used as the reference gene to normalize target genes of interest.

Western blot. Liver tissue was homogenized in Tissue Protein Extraction Reagent (T-PER®, Waltham, Massachusetts, USA). Equal amounts of protein were loaded onto Criterion Tris-HCl gels (Bio-Rad Lab, Hercules, CA) and electro-transferred to Immobilion® - FL PVDF membrane (EMD Millipore). The membranes were blocked in either 5% Non-Fat Dry Milk or 5% bovine serum albumin in TBST depending on the primary antibody manufacturer's recommendation for 1 hour at room temperature. Membranes were then incubated with the primary antibody overnight followed by incubation with horseradish peroxidase-conjugated secondary antibodies for 1 hour. Pierce ECL Western Blotting Substrate (ThermoFisher Scientific, Waltham, Massachusetts, USA) was used to detect the HRP activity of the secondary antibodies and expose to films. Primary antibodies used were: phopsho-PERK (Product # 3179), total PERK (Product # 3192), phospho-eIF2α (9721), and total eIF2α (9722) from Cell Signaling Technology, ATF4 (sc-200) and CHOP (sc-7351) from Santa Cruz Biotechnology, GAPDH (Millipore, Mab374) and alpha-tubulin (Sigma, T9026).

Bone Marrow Derived Macrophage (BMDM) isolation and assays. BMDM were isolated from the hind bones of mice. Bone marrow was flushed out of the bones using HEPES balanced salt solution, dissociated via passing through a 25 gauge needle twice and plated in petri dishes in RPMI containing 20% L929 cell-conditioned medium, 10% fetal bovine serum and incubated at 37°C in 5% CO_2. BMDMs were dissociated after 7 days of differentiation using Accutase.

Migration assays were conducted in modified Boyden chambers. Cells were pelleted at 1500 rpm for 5 minutes at 4°C, resuspended in serum-free RPMI, plated into 60-mm dishes in complete medium. Treatment media was made next day using RPMI containing 2% FBS. Media was removed from the 60-mm dishes, cells were gently rinsed with PBS and 3 mL of

treatment media was placed on for 1 hour as a preincubation step. Meanwhile, filters were evenly coated with 0.1% gelatin/PBS at room temperature for 25 minutes and dried for another 35 minutes. Cells were removed following the preincubation step, counted and diluted to 2,500,000 cells/ml. 220 μL of lipopolysaccharide (10 ng/mL) was placed at the bottom and cells on the top of the assembled chamber. Cells were allowed to migrate for 3 hours following which excess cells and media were removed from the top chamber, the chamber was disassembled to collect the filter papers. Filter papers were fixed in 10% formaldehyde for 30 minutes at room temperature, washed in PBS and inverted with migrated cell side down on to a labelled glass slide with a drop of Anti-fade GOLD with DAPI. Slides were left overnight to cure, sealed and examined under confocal microscopy to count the number of migrated cells.

Data availability. All data generated or analyzed during this study are included in this published article (and its Supplementary Information files).

Statistical and data analyses. Data are presented as mean ± S.E.M. The students two-tailed t-test was used for comparing groups. Statistical analyses were performed in GraphPad Prism version 7.00 for Windows, GraphPad Software, LaJolla, CA, USA, www.graphpad.com. A p value of < 0.05 was considered significant.

ACKNOWLEDGEMENTS

The authors are grateful to Dr. M.G. Katze for the generous gift of *p58*$^{ipk-/-}$ mice and Ms. Courtney Hoover for superb administrative assistance. The mouse metabolic phenotyping core acknowledges the generous support of the Robert and Arlene Kogod Center on Aging.

AUTHOR CONTRIBUTIONS STATEMENT

The experiments were designed and conducted by H.B., D.D., A.S.M., and H.M. Experiments were conducted by H.B., D.D., A.S.M., B.N, R.P.G., S.K., P.H. and H.M. H.M. and H.B. wrote the main manuscript text. H.B. prepared figures 1-9. All authors reviewed the manuscript.

REFERENCES

1 Rinella, M. E. Nonalcoholic fatty liver disease: a systematic review. *JAMA* **313**, 2263-2273, doi:10.1001/jama.2015.5370 (2015).

2 Hirsova, P., Ibrabim, S. H., Gores, G. J. & Malhi, H. Lipotoxic lethal and sublethal stress signaling in hepatocytes: relevance to NASH pathogenesis. *J Lipid Res* **57**, 1758-1770, doi:10.1194/jlr.R066357 (2016).

3 Volmer, R., van der Ploeg, K. & Ron, D. Membrane lipid saturation activates endoplasmic reticulum unfolded protein response transducers through their transmembrane domains. *Proc Natl Acad Sci U S A* **110**, 4628-4633, doi:10.1073/pnas.1217611110 (2013).

4 Lin, J. H., Li, H., Zhang, Y., Ron, D. & Walter, P. Divergent effects of PERK and IRE1 signaling on cell viability. *PLoS One* **4**, e4170, doi:10.1371/journal.pone.0004170 (2009).

5 Ron, D. & Walter, P. Signal integration in the endoplasmic reticulum unfolded protein response. *Nat Rev Mol Cell Biol* **8**, 519-529, doi:10.1038/nrm2199 (2007).

6 Malhi, H. *et al.* C/EBP homologous protein-induced macrophage apoptosis protects mice from steatohepatitis. *J Biol Chem* **288**, 18624-18642, doi:10.1074/jbc.M112.442954 (2013).

7 Ji, C. *et al.* Liver-specific loss of glucose-regulated protein 78 perturbs the unfolded protein response and exacerbates a spectrum of liver diseases in mice. *Hepatology* **54**, 229-239, doi:10.1002/hep.24368 (2011).

8 Lee, A. H., Scapa, E. F., Cohen, D. E. & Glimcher, L. H. Regulation of hepatic lipogenesis by the transcription factor XBP1. *Science* **320**, 1492-1496, doi:10.1126/science.1158042 (2008).

9 Liu, X. *et al.* Hepatic deletion of X-box binding protein 1 impairs bile acid metabolism in mice. *J Lipid Res* **58**, 504-511, doi:10.1194/jlr.M071266 (2017).

10 van Huizen, R., Martindale, J. L., Gorospe, M. & Holbrook, N. J. P58IPK, a novel endoplasmic reticulum stress-inducible protein and potential negative regulator of eIF2alpha signaling. *J Biol Chem* **278**, 15558-15564, doi:10.1074/jbc.M212074200 (2003).

11 Nakamura, T. *et al.* Double-stranded RNA-dependent protein kinase links pathogen sensing with stress and metabolic homeostasis. *Cell* **140**, 338-348, doi:10.1016/j.cell.2010.01.001 (2010).

12 Rutkowski, D. T. *et al.* The role of p58IPK in protecting the stressed endoplasmic reticulum. *Mol Biol Cell* **18**, 3681-3691, doi:10.1091/mbc.E07-03-0272 (2007).

13 Tan, S. L., Gale, M. J., Jr. & Katze, M. G. Double-stranded RNA-independent dimerization of interferon-induced protein kinase PKR and inhibition of dimerization by the cellular P58IPK inhibitor. *Mol Cell Biol* **18**, 2431-2443 (1998).

14 Roobol, A. *et al.* p58IPK is an inhibitor of the eIF2alpha kinase GCN2 and its localization and expression underpin protein synthesis and ER processing capacity. *Biochem J* **465**, 213-225, doi:10.1042/BJ20140852 (2015).

15 Korth, M. J., Lyons, C. N., Wambach, M. & Katze, M. G. Cloning, expression, and cellular localization of the oncogenic 58-kDa inhibitor of the RNA-activated human and mouse protein kinase. *Gene* **170**, 181-188 (1996).
16 Ladiges, W. C. *et al.* Pancreatic beta-cell failure and diabetes in mice with a deletion mutation of the endoplasmic reticulum molecular chaperone gene P58IPK. *Diabetes* **54**, 1074-1081 (2005).
17 Mauer, A. S., Hirsova, P., Maiers, J. L., Shah, V. H. & Malhi, H. Inhibition of Sphingosine 1-phosphate Signaling Ameliorates Murine Nonalcoholic Steatohepatitis. *Am J Physiol Gastrointest Liver Physiol*, ajpgi 00222 02016, doi:10.1152/ajpgi.00222.2016 (2016).
18 Haataja, L., Gurlo, T., Huang, C. J. & Butler, P. C. Many commercially available antibodies for detection of CHOP expression as a marker of endoplasmic reticulum stress fail specificity evaluation. *Cell Biochem Biophys* **51**, 105-107, doi:10.1007/s12013-008-9019-2 (2008).
19 Yan, W. *et al.* Control of PERK eIF2alpha kinase activity by the endoplasmic reticulum stress-induced molecular chaperone P58IPK. *Proc Natl Acad Sci U S A* **99**, 15920-15925, doi:10.1073/pnas.252341799 (2002).
20 Synofzik, M. *et al.* Absence of BiP co-chaperone DNAJC3 causes diabetes mellitus and multisystemic neurodegeneration. *Am J Hum Genet* **95**, 689-697, doi:10.1016/j.ajhg.2014.10.013 (2014).
21 Takata, K. *et al.* Comparison of energy metabolism in insulin-dependent and non-insulin-dependent diabetes mellitus. *J Med Invest* **44**, 67-71 (1997).
22 Buscemi, S. *et al.* Resting energy expenditure in type 2 diabetic patients and the effect of insulin bolus. *Diabetes Res Clin Pract* **106**, 605-610, doi:10.1016/j.diabres.2014.09.016 (2014).
23 Muller, M. J. *et al.* Energy expenditure in children with type I diabetes: evidence for increased thermogenesis. *BMJ* **299**, 487-491 (1989).
24 Feldstein, A. E. *et al.* Hepatocyte apoptosis and fas expression are prominent features of human nonalcoholic steatohepatitis. *Gastroenterology* **125**, 437-443 (2003).
25 Morinaga, H. *et al.* Characterization of distinct subpopulations of hepatic macrophages in HFD/obese mice. *Diabetes* **64**, 1120-1130, doi:10.2337/db14-1238 (2015).
26 Idrissova, L. *et al.* TRAIL receptor deletion in mice suppresses the inflammation of nutrient excess. *J Hepatol* **62**, 1156-1163, doi:10.1016/j.jhep.2014.11.033 (2015).
27 Deldicque, L. *et al.* The unfolded protein response is activated in skeletal muscle by high-fat feeding: potential role in the downregulation of protein synthesis. *Am J Physiol Endocrinol Metab* **299**, E695-705, doi:10.1152/ajpendo.00038.2010 (2010).
28 Cao, J. *et al.* Saturated fatty acid induction of endoplasmic reticulum stress and apoptosis in human liver cells via the PERK/ATF4/CHOP signaling pathway. *Mol Cell Biochem* **364**, 115-129, doi:10.1007/s11010-011-1211-9 (2012).
29 Harding, H. P. *et al.* Diabetes mellitus and exocrine pancreatic dysfunction in perk-/- mice reveals a role for translational control in secretory cell survival. *Mol Cell* **7**, 1153-1163 (2001).
30 Brunt, E. M. *et al.* Nonalcoholic fatty liver disease (NAFLD) activity score and the histopathologic diagnosis in NAFLD: distinct clinicopathologic meanings. *Hepatology* **53**, 810-820, doi:10.1002/hep.24127 (2011).

Figure 1

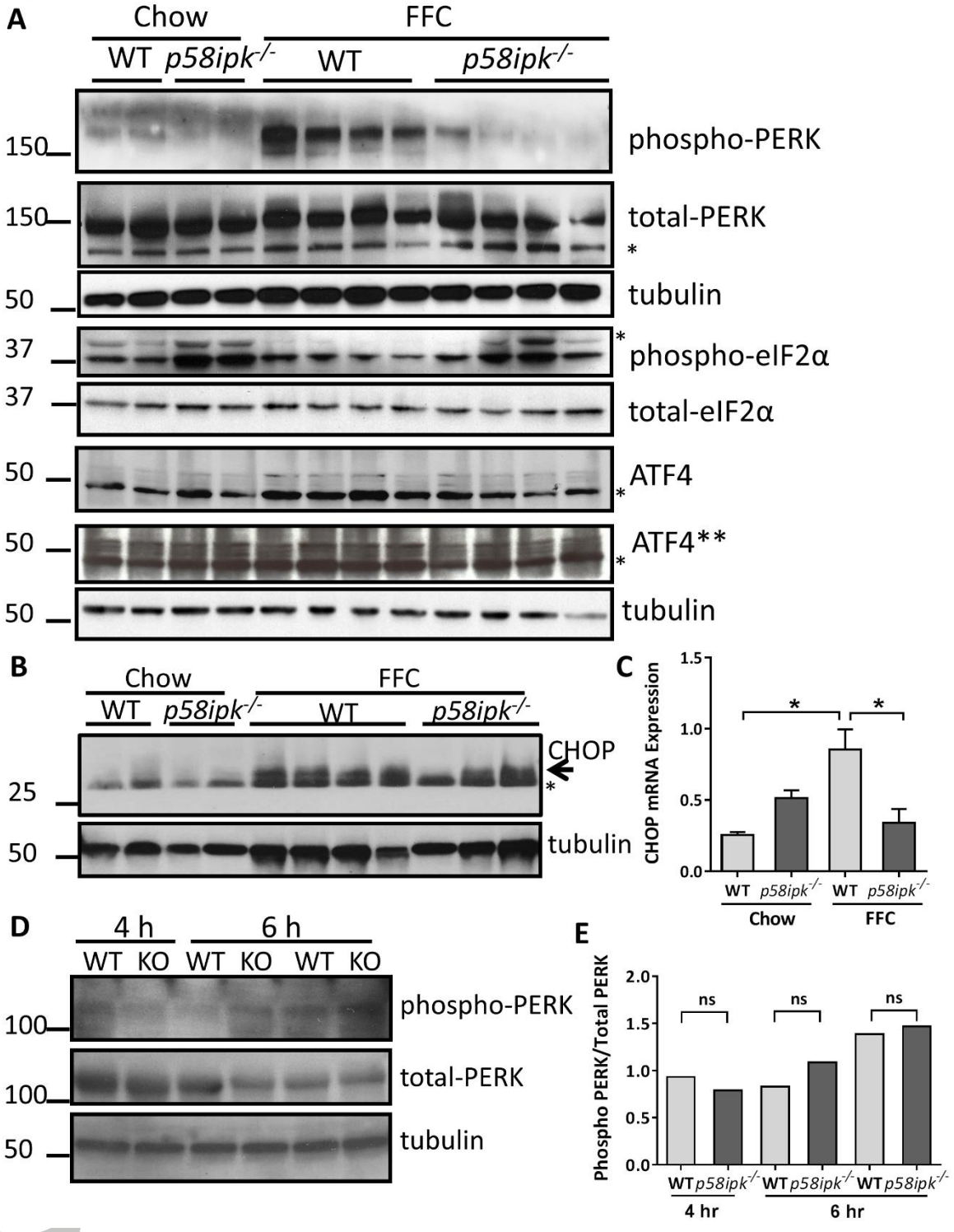

Figure 1. PERK activation is attenuated in FFC-fed *p58$^{ipk-/-}$* mice. A) Western blot images from chow-fed (n=2 per genotype) and FFC-fed (n=4 per genotype) wild type and *p58$^{ipk-/-}$* mice are shown. Phospho-PERK, total PERK, phospho-eIF2α, total-eIF2α, ATF4 and tubulin expression were examined in liver lysates. The asterisk denotes non-specific band. ATF4** is

a longer exposure of ATF4. B) Western blot images from chow-fed (n=2 per genotype) and FFC-fed (n=4 WT and n=3 *p58*$^{ipk-/-}$) treated mouse livers are shown. Expression of CHOP and tubulin were examined in liver lysates. The asterisk denotes non-specific band. C) Relative mRNA expression of CHOP in all 4 groups of mice expressed relative to chow-fed WT mice, * $p<0.05$ D) Phospho-PERK, total PERK and tubulin expression in liver lysates following intraperitoneal tunicamycin injection. Three wild type (WT) and 3 *p58*$^{ipk-/-}$ (KO) mice were included. E) The densitometry results of the Western blot of Figure 1D are shown as a bar graph. ns, not significant.

Figure 2

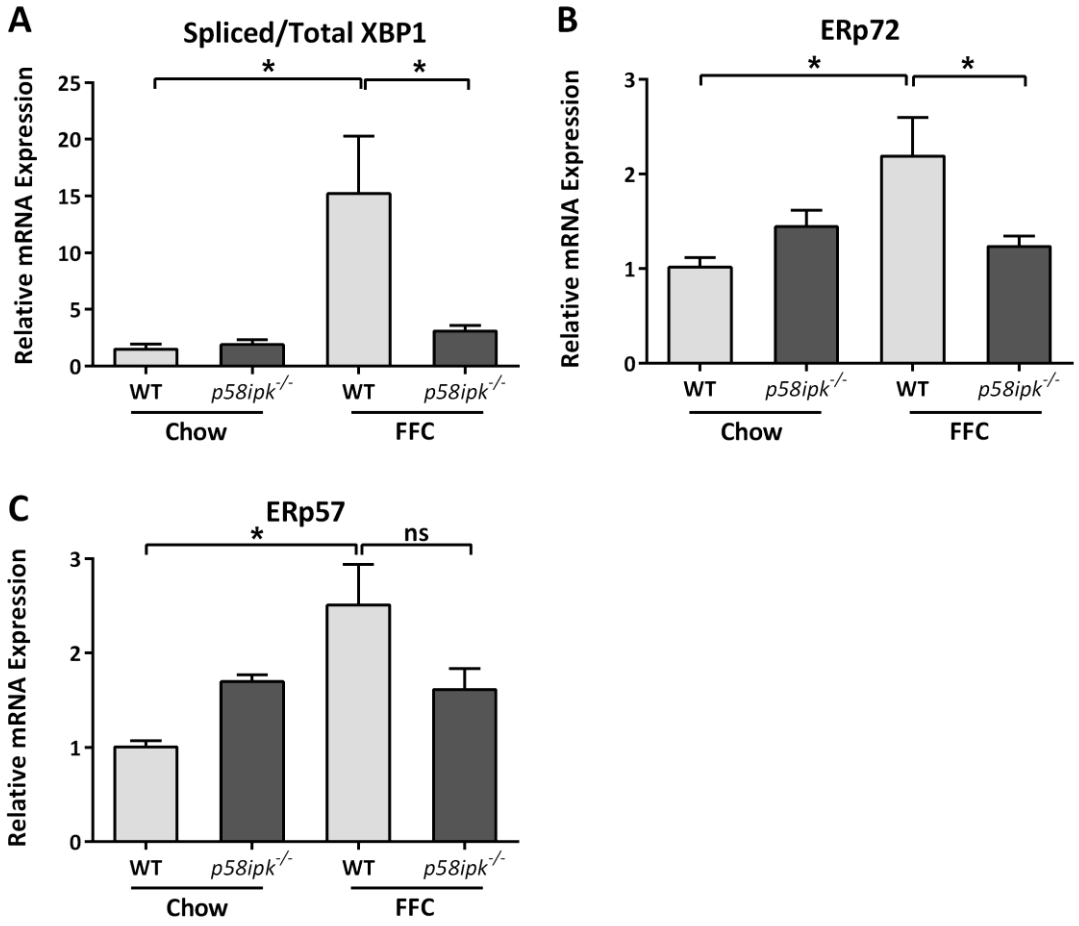

Figure 2. FFC-fed p58$^{ipk-/-}$ mice show reduced ER stress response. A) Relative mRNA expression of Spliced XBP1 and Total XBP1 in all 4 groups of mice expressed relative to chow-fed WT mice, * $p<0.05$. B) Relative mRNA expression of Endoplasmic Reticulum Resident Protein 57 (ERp57) in all 4 groups of mice expressed relative to chow-fed WT mice, * $p<0.05$. ns, non-significant. C) Relative mRNA expression of Endoplasmic Reticulum Resident Protein 72 (ERp72) in all 4 groups of mice expressed relative to chow-fed WT mice, * $p<0.05$.

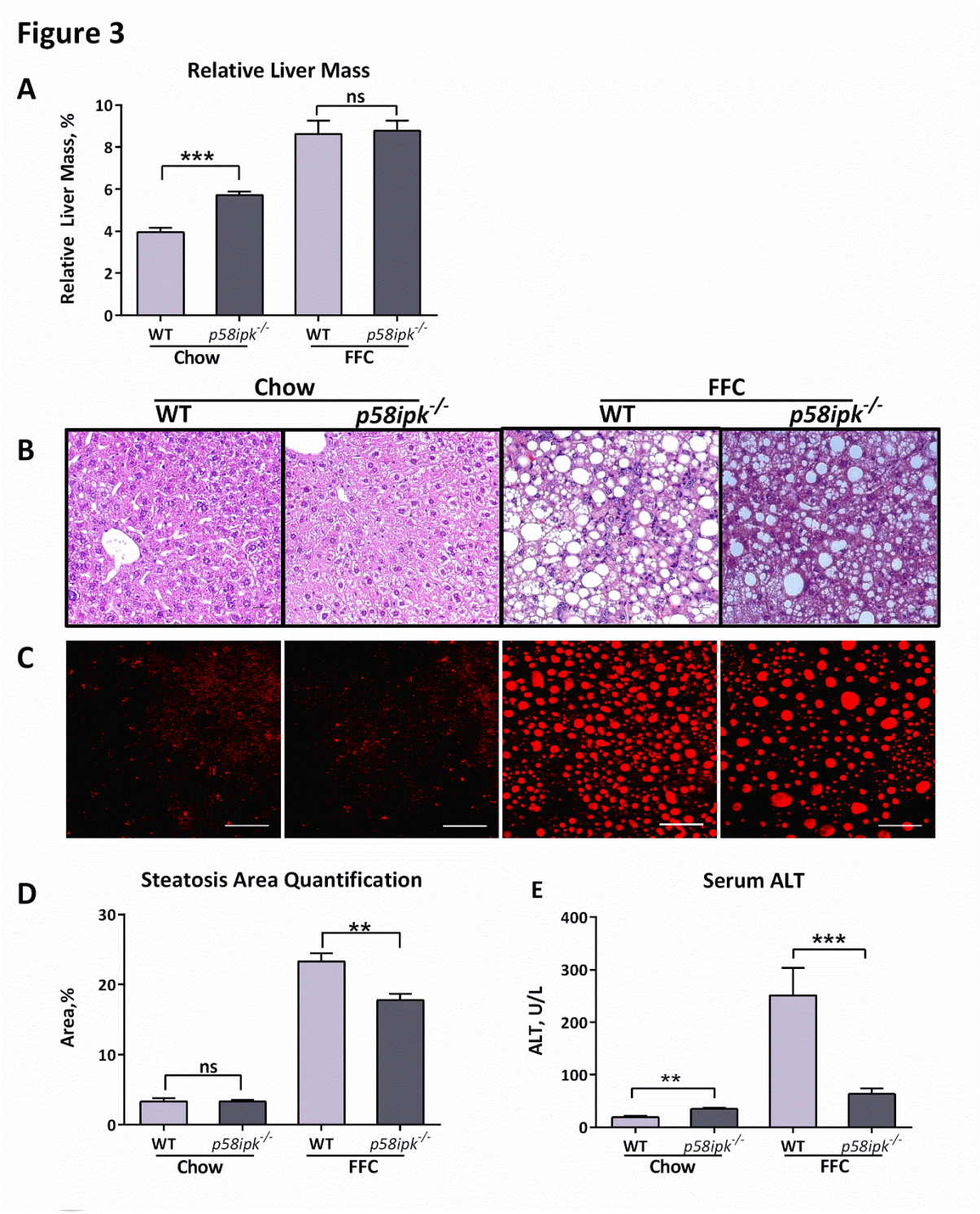

Figure 3. *P58*$^{ipk-/-}$ mice are protected from NASH. A) Relative liver mass was calculated as a ratio of absolute liver mass to body mass and expressed as % body mass, (n = 6-8) ***p<0.001. B) Standard Histology by H&E from each of the 4 groups. C) CARS microscopy for assessment of neutral triglyceride and D) its quantification, (n = 5 each) **p = 0.0054. E) Serum alanine aminotransferase (ALT) was in (n = 6-8), **p = 0.0010, ***p = 0.0031. ns, non-significant.

Figure 4

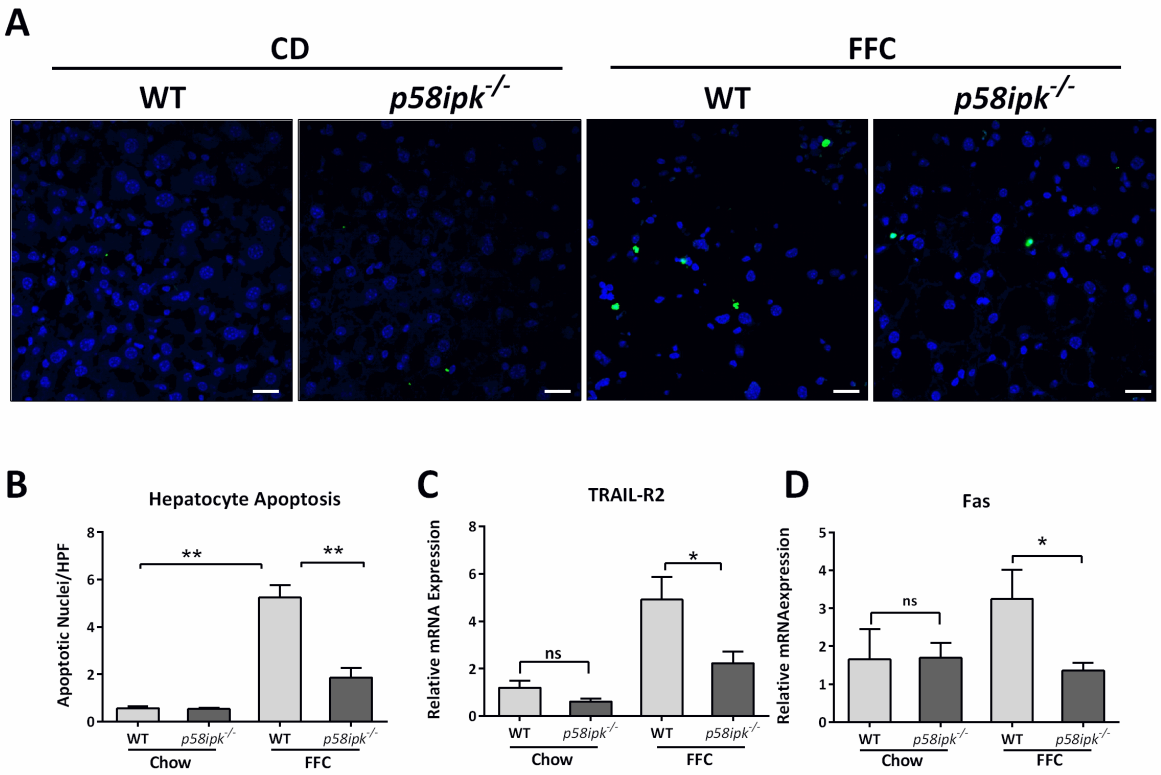

Figure 4. *P58*^{ipk} deletion protects against hepatocyte apoptosis in NASH. A) Fluorescent TUNEL assay was performed on cryosections from (n = 4 each, chow-fed WT and knockout, n = 5 each, FFC-fed WT and knockout) followed by DAPI nuclear counterstain. Scale bar = 20 μM. B) Hepatocyte apoptosis was quantified by the measurement of the number of apoptotic nuclei/high-power field (HPF) for at least 10 HPFs (n = 4 each, chow-fed WT and knockout, n = 5 each, FFC-fed WT and knockout), **p<0.01. C) Relative mRNA expression of TRAIL-R2 in all 4 groups of mice expressed relative to chow-fed WT (n = 5-6), **p = 0.0225. D) Relative mRNA expression of Fas expressed relative to chow-fed WT (n = 5-6), * p = 0.0313. ns, non-significant.

Figure 5

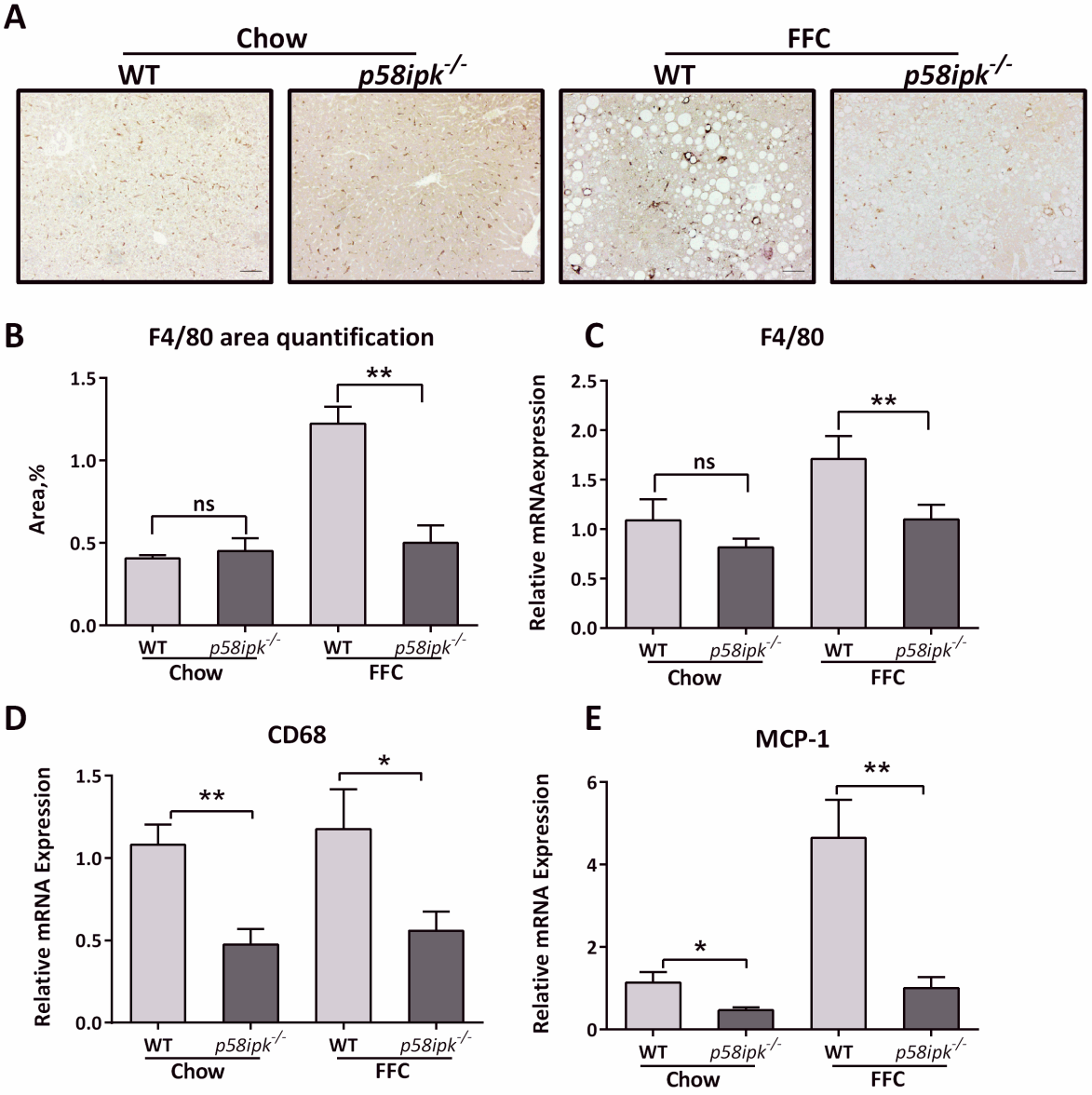

Figure 5. Liver inflammation in reduced in FFC-fed *p58*$^{ipk-/-}$ mice. A) Representative F4/80 immunohistochemistry from each of the 4 groups is shown (n = 4 each, chow-fed WT and knockout, n = 5 each, FFC-fed WT and knockout). B) Quantification of F4/80 immunohistochemistry, **p = 0.0026. C) Relative mRNA expression of F4/80 in all 4 groups of mice expressed relative to chow-fed WT mice (n = 4-5 per group), **p < 0.01. D) Relative mRNA expression of CD68 in all 4 groups of mice expressed relative to chow-fed WT mice, *p<0.05, **p < 0.01. ns, non-significant. E) Relative mRNA expression of monocyte chemotactic protein 1 (MCP-1) in all 4 groups of mice expressed relative to chow-fed WT mice (n=4-5), *p<0.05, **p < 0.01.

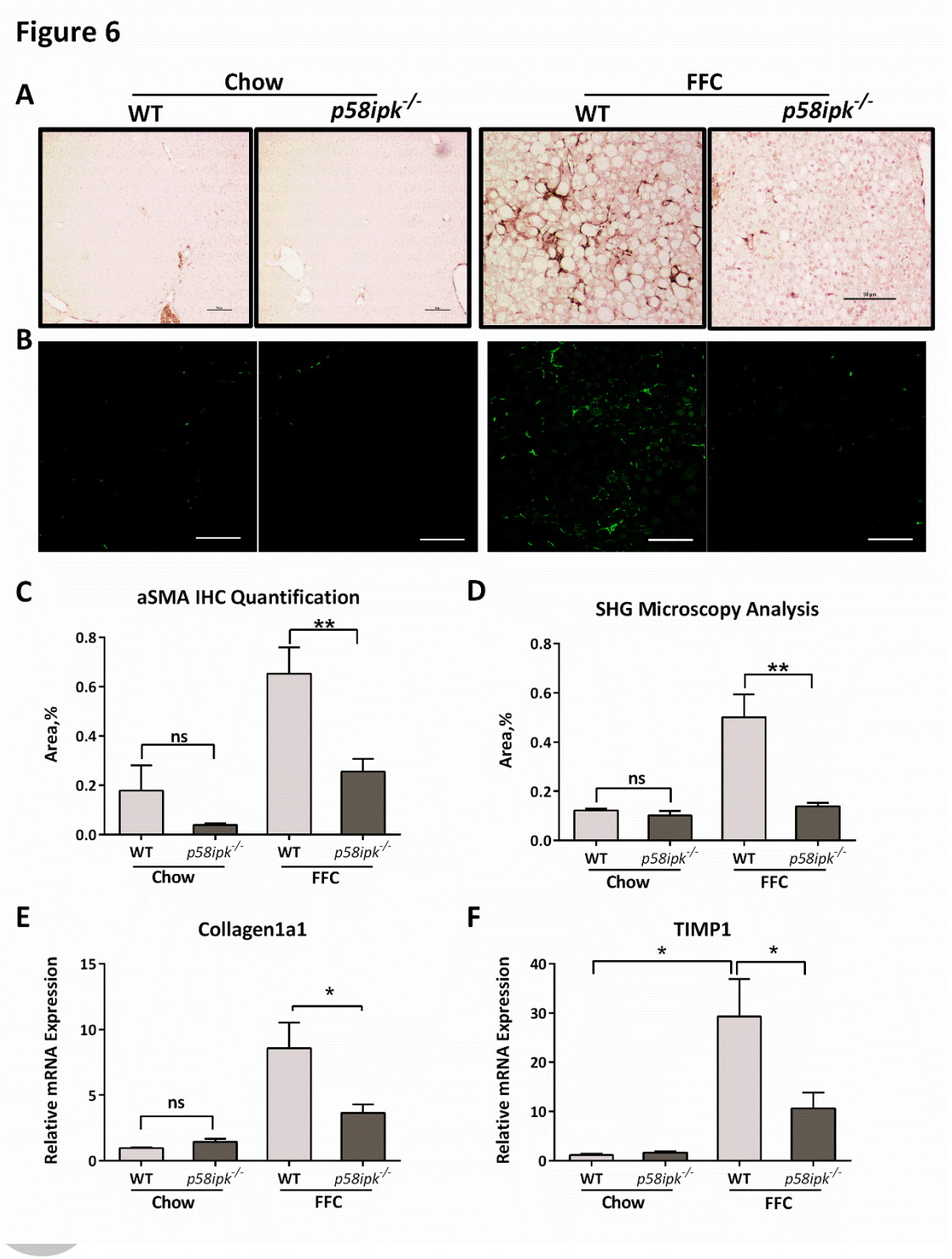

Figure 6. Hepatic fibrosis is reduced in FFC-fed *p58$^{ipk-/-}$* mice. A) Representative images of alpha smooth muscle actin (aSMA) immunohistochemistry from each of the 4 groups is shown (n = 6). B) Representative photomicrographs of collagen visualization by second harmonic generation microscopy are shown. C) Alpha-SMA immunohistochemistry area quantification (n = 6), **p = 0.0072. D) Quantification of collagen content detected by second harmonic generation microscopy (n = 5), ** p = 0.0048. E) Relative mRNA expression of collagen1a1 (n = 5-8) and F) tissue inhibitor of metalloproteinase 1 (TIMP1) (n = 5-8) in all groups expressed relative to chow-fed WT mice. *p< 0.05. ns, non-significant.

Figure 7

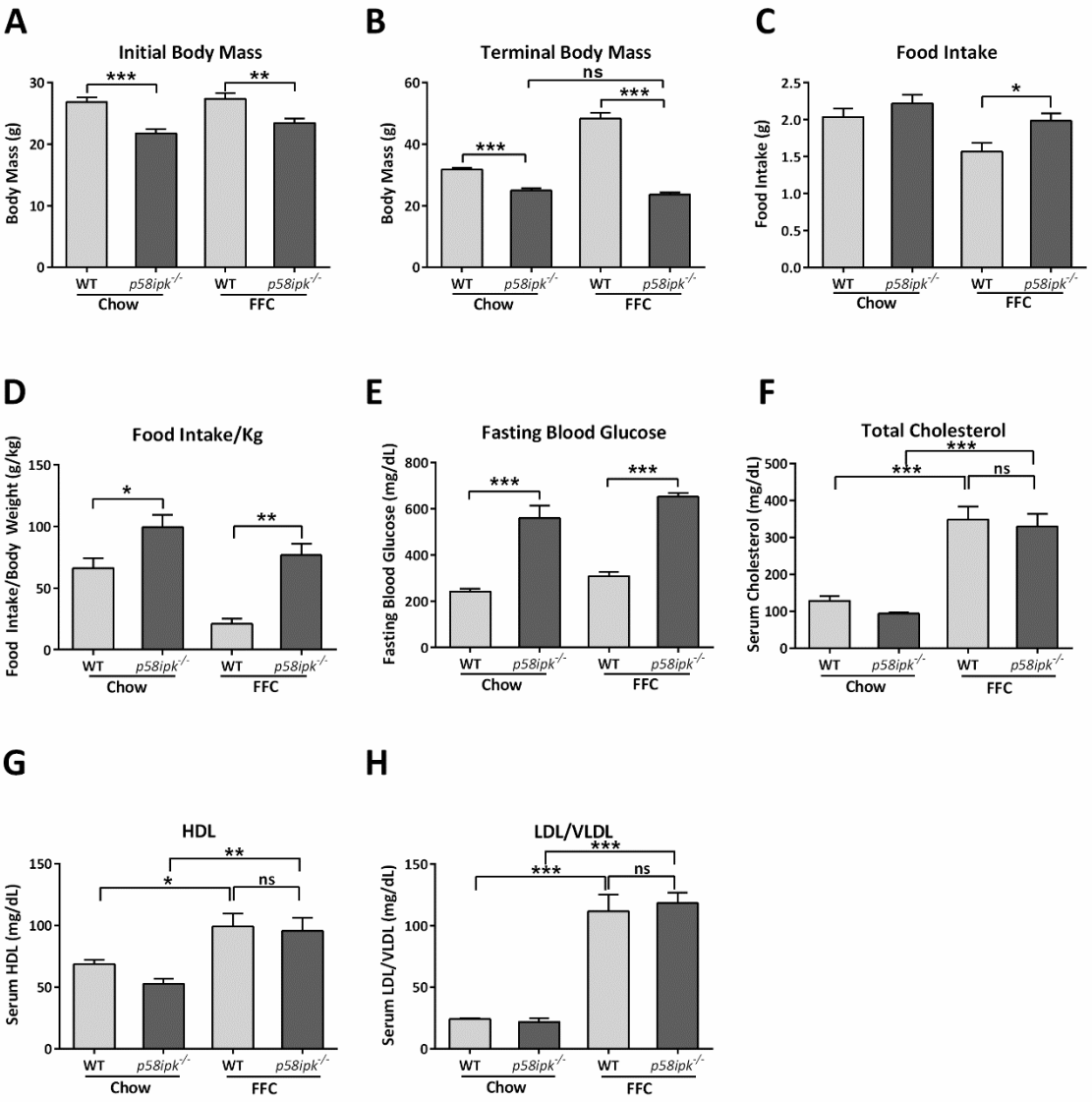

Figure 7. *P58*$^{ipk-/-}$ mice are resistant to diet-induced obesity. A) Initial body mass in grams measured at the start of the feeding study (n= 6-8), ***p = 0.0004, **p = 0.0045. B) Terminal body mass in grams following 20 weeks of chow or FFC feeding (n = 6-8), ***p < 0.0001. C) Food intake in grams was measured in 4 mice per group during CLAMS, **p = 0.037and D) Food intake per kg (n = 4), *p = 0.038, **p = 0.001. E) Fasting blood glucose from all 4 groups, (n = 6-8), *** p<0.001. ns, non-significant. F) Total Cholesterol concentration from all 4 groups (n = 4-9), *** p<0.001. ns, non-significant. G) Serum HDL concentration from all 4 groups (n = 5-7), *p = 0.02, ** p = 0.008. ns, non-significant. H) Serum LDL concentration from all 4 groups (n = 5-7), *** p<0.001. ns, non-significant.

Figure 8

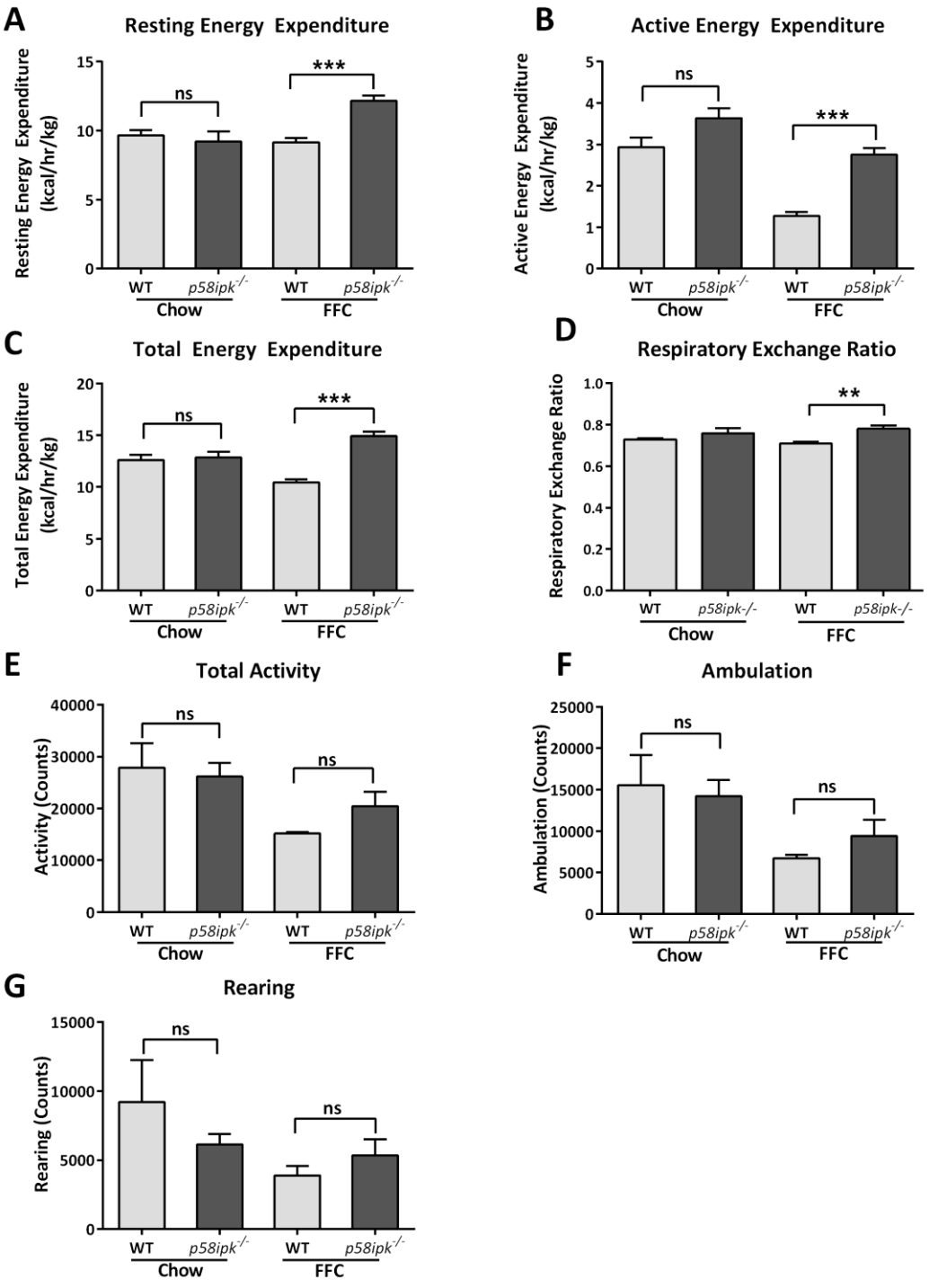

Figure 8. Energy expenditure is increased in FFC-fed *p58$^{ipk-/-}$* mice. A) Resting energy expenditure, B) Active energy expenditure, C) Total energy expenditure, D) Respiratory exchange ratio in the fasted state, E) Total activity, F) Ambulation and G) Rearing from 4 mice each per group were assessed by CLAMS. *p <0.05, **p<0.05, ***p<0.001. ns, non-significant.

Figure 9

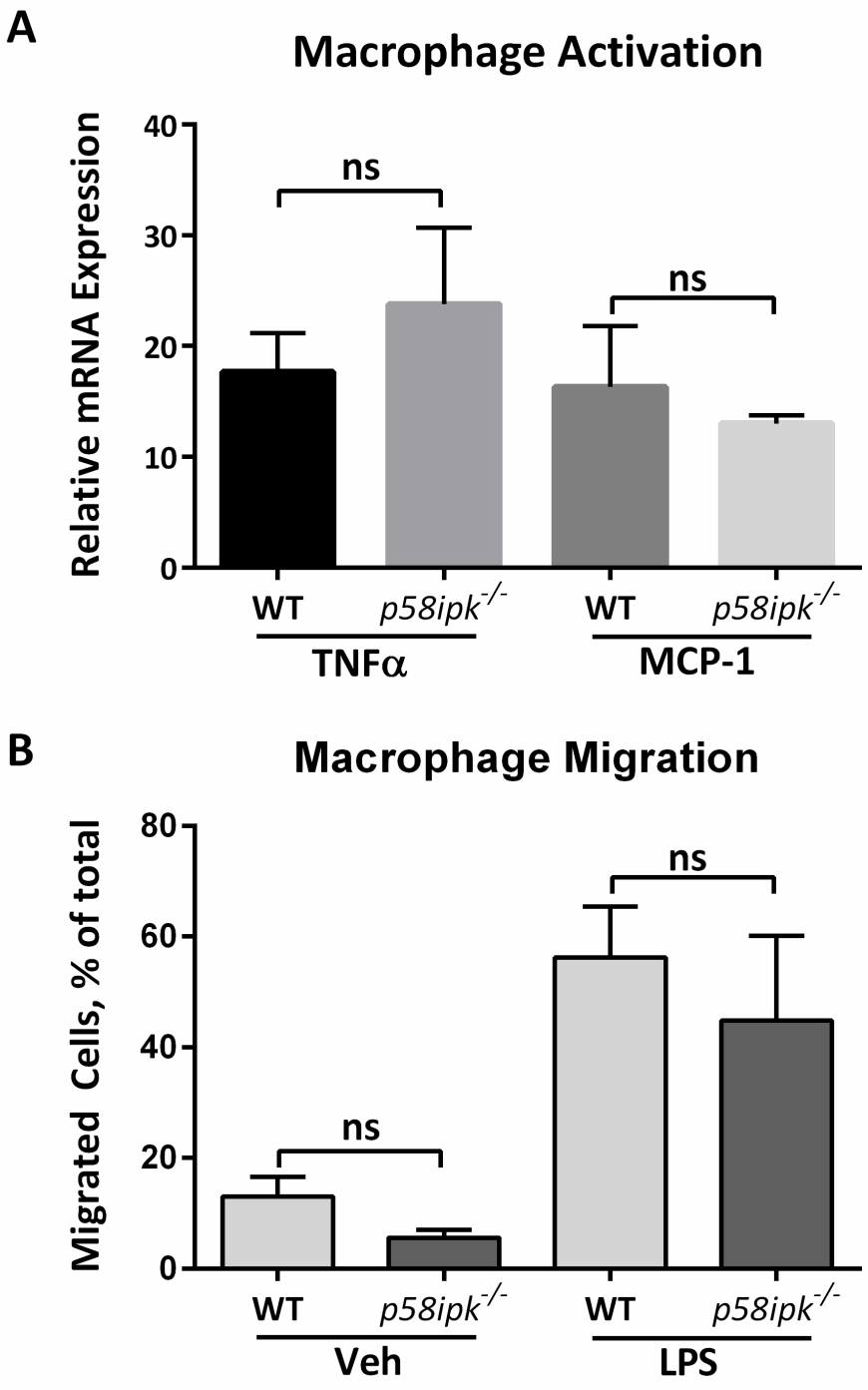

Figure 9. Proinflammatory and migratory response are intact in *p58*$^{ipk-/-}$ macrophages. A) Proinflammatory responses in WT or *p58*$^{ipk-/-}$ bone marrow derived macrophages (BMDM) were measured by qPCR for mRNA expression for tumor necrosis factor alpha (TNFα) and monocyte chemotactic protein 1 (MCP-1) following treatment with 10 ng/mL LPS for 6 hours. Data are expressed relative to vehicle treated controls (n = 3). B) BMDM from WT or *p58*$^{ipk-/-}$ mice were let migrate toward vehicle or 10 ng/mL LPS for 3 hours (n = 3). ns, non-significant.

Table 1. Sequences of primers used for qPCR

Gene	Forward Sequence	Reverse Sequence
HPRT	5-TCCTCCTCAGACCGCTTTT-3	5-TCCTCCTCAGACCGCTTTT-3
Col1A1	5-GCTCCTCTTAGGGGCCAC-3	5-CCACGTCTCACCATTGGGG-3
TIMP1	5-AGGTGGTCTCGTTGATTTCT-3	5-GTAAGGCCTGTAGCTGTGCC-3
MCP-1	5-TTAAAAACCTGGATCGGAACCAA-3	5-GCATTAGCTTCAGATTTACGGGT-3
F4/80	5-ATGGACAAACCAACTTTCAAGGC-3	5-GCAGACTGAGTTAGGACCACAA-3
CD68	5-TGTCTGATCTTGCTAGGACCG-3	5-GAGAGTAACGGCCTTTTTGTGA-3
TRAIL-R2	5-CGGGCAGATCACTACACCC-3	5-TGTTACTGGAACAAAGACAGCC-3
Fas	5-TATCAAGGAGGCCCATTTTGC-3	5-TGTTTCCACTTCTAAACCATGCT-3
Ddit3 (CHOP)	5-CTGCCTTTCACCTTGGAGAC-3	5-CGTTTCCTGGGGATGAGATA-3
XBP-1 spliced	5-AAGAACACGCTTGGGAATGG-3	5-CTGCACCTGCTGCGGAC-3
XBP-1 total	5-GTCCATGGGAAGATGTTCTGG-3	5-TGGCCGGGTCTGAGTCCG-3
ERp57	5-CGCCTCCGATGTGTTGGAA-3	5-CAGTGCAATCCACCTTTGCTAA-3
ERp72	5-TCCCATTGCTGTAGCGAAGAT-3	5-GGGGTAGCCACTCACATCAAAT-3